Synthesis and Characterization of the Rare-Earth Chloride Complexes with *N,N,N′,N′*-Tetramethylmalonamide

Dmytro V. Kravchuk and Richard E. Wilson*

Chemical Sciences and Engineering Division, Argonne National Laboratory, 9700 S Cass Ave Lemont, IL 60439 United States

Abstract

Exploration of the solid-state chemistry of the *f*-elements and their coordination chemistry can assist in understanding the speciation of these elements in solution, which, in turn, can aid in the interpretation of their chemical behavior in complex liquid-liquid separations. Within these separation processes, malonamides are common organic extractants that are used for complexing both lanthanides and actinides, thus it is relevant to understand the malonamide ligand complexation under various conditions. In this work, we investigate solid-state complexes of the rare-earth chlorides with *N,N,N′,N′*-tetramethylmalonamide (TMMA) across the entire lanthanide series. We isolated two structural families of compounds $Ln(TMMA)_2Cl_3$ Ln = La-Dy and $[Ln(TMMA)_2(H_2O)_4]Cl_3 \bullet xH_2O$ x = 0,4 Ln = Ho-Lu, showing differences in chloride coordination from the inner-sphere complex for early lanthanides to outer-sphere for the late lanthanides. Both structural series were additionally analyzed by both IR and Raman spectroscopy confirming similarities in malonamide ligand coordination modes, while showing differences in vibrational features associated with chloride and aqua ligand coordination.

Introduction

Coordination chemistry, and the correlation of a metal ion's coordination chemistry and structure is an important component in describing the energy landscape associated with chemical separations. Effective separation of heavy elements from acidic aqueous media is typically achieved using bifunctional organic extractants in an immiscible organic solvent within liquid-liquid separation processes.[1] Among the commonly used extracting agents, diamide/malonamide-based extractants are showing promise in hydrometallurgical processes such as the selective actinide extraction (DIAMEX-SANEX), due to their ability to batch extract all trivalent lanthanides and actinides into the organic phase at once.[2, 3] Malonamides are also proposed as co-extractants with tributylphosphate (TBP) in a new EURO-GANEX process aimed at homogeneous recovery of transuranic elements following an initial uranium extraction cycle.[4, 5] The growing relevance of diamide extractants brought about numerous reports investigating the distribution ratios and speciation of malonamides with both lanthanides and actinides in liquid-liquid extraction systems to understand and improve the efficacy of heavy element separations.[6] Such investigations typically relied on extended X-ray absorption fine structure (EXAFS) or small angle X-ray scattering (SAXS) techniques to elucidate the coordination sphere of the metal ions, yet the resulting coordination numbers were imprecise and the exact metal speciation in solution remains unknown.[7]

Studying the coordination chemistry of *f*-elements in the solid state offers an alternative approach to exploring the diamide binding to the metal center, providing solid state models of their coordination chemistry and potentially addressing the limitations of the previously used spectroscopic and scattering techniques.[8] In the context of coordination chemistry, the neutral malonamide ligand is particularly interesting as it can successfully outcompete coordinated solvent molecules for a binding site on the metal center.[9] Malonamide binding is favorable due to the chelation effect as a result of the bidentate ligand coordination through both C=O oxygens of the diamide functional group, as first shown by Castellano and Becker in the $[La(K^2\text{-TMMA})_4](PF_6)_3$ complex.[10] In the case of secondary or primary amide, the

lack of steric hindrance on the unsubstituted *N,N′*-malonamides allows the carbonyl groups to take on *trans* conformation resulting in a rare μ_2-O,O′ bridging motif, as later shown by Kannan and Ferguson in $[(UO_2((C_6H_5CO)_2CH)_2)_2(\mu_2\text{-}(C_6H_5NHCO)_2CH_2)]$.[11] Such synthetic tunability of the malonamide molecule allows for a fine control of the alkyl substituents or the modifications to the carbon backbone affecting solubility, conformation, and preorganization of the ligand, in turn improving the separation factors during extraction experiments and diversifying the library of the isolated *f*-element-malonamide solid-state compounds.

The first examples of synthetically modified diamides were presented by Drew *et al*., who showed that treating dimethyl malonate with an appropriate disubstituted amine yields *N,N′*-diphenyl-*N,N′*-dimethylmalonamides (dmpma) and *N,N′*-dicyclohexyl-*N,N′*-dimethylmalonamide (dcmma), which were then used in the reactions with neodymium and ytterbium resulting in a 10-coordinate $[Nd(dmpma)(NO_3)_3(H_2O)_2]$ and a 9-coordinate $[Yb(dmpma)(NO_3)_3(H_2O)]$ in the case of phenyl substitution, as well as $[Nd(dcmma)_2(NO_3)_3]$ in case of cyclohexyl substitution.[12] Soon thereafter, Drew *et al*. expanded on their initial findings by modifying the carbon backbone of the malonamide ligand with butyl and ethoxy ethyl groups attached to the methylene carbon, as evidenced by crystallized Nd and Pr complexes, respectively.[13] Separately, Lumetta *et al*. considered how the conformational substructure of the malonamide (i.e. *cis*, *trans*, or *gauche* of the neighboring C=O) complements the binding affinity of the malonamide ligand and suggested the bicyclic backbone modification.[14] Such synthetic adjustment was later implemented by Parks *et al*. who isolated structural pairs of Nd and Gd with both *N,N,N′,N′*-tetramethylmalonamide (TMMA) and its bicyclic analogue in the solid state, while the solution studies showed 10-100 fold increase in binding affinity of the bicyclic malonamide extractant with Ln(III) compared to the acyclic counterpart.[15] A recent structural report of synthetically modified malonamides by Tyumentsev *et al*. adopted a polydentate approach by attaching several malonamide ligands to a "platform" phenyl ring, thus forming a bismalonamide derivative with multiple metal binding sites. Instead of coordination to a central lanthanide metal center, the resulting bismalonamides preferred a

bridging mode across multiple metal centers allowing for isolation of multiple neodymium dimers in the solid-state.[16]

A broad survey of the *f*-element-malonamide solid-state structures reveals that the common feature across all reported structures in the Cambridge Crystallographic Database to date is the presence of nitrate as a counter-anion. Incorporation of nitrate is reasonable since most employed liquid-liquid extraction processes occur between the ~3M HNO_3 aqueous media and the aliphatic phase, thus the speciation of the extracted metal would contain both malonamide and nitrato ligands forming a charge-neutral complex.[17, 18] Yet, if we look at the early ion-exchange studies of trivalent lanthanides and actinides by Seaborg and coworkers, the use of chloride as a soft-donor ligand showed significant variability in elution rates of An(III) compared to Ln(III) as a function of hydrochloric acid concentration, suggesting a basis for soft donor separation process.[19, 20] In this work, we aim to explore the crossover between the soft-donor chloride and the malonamide ligand in the solid-state structures across the entire lanthanide series benchmarked with our earlier studies of the nitrate system.[8] We report synthesis and isolation of lanthanide bismalonamide complexes with inner-sphere coordinated chloride $Ln(TMMA)_2Cl_3$ as an isostructural series from La to Dy, that undergo a structural change to an outer-sphere chloride complexes $[Ln(TMMA)_2(H_2O)_4]Cl_3 \bullet xH_2O$ $x = 0,4$ for the later lanthanides Ho-Lu. We provide complementary IR and Raman spectroscopic analysis and make structural comparisons of the newly isolated chloride series to their nitrate counterparts reported in the literature. Such coordination compounds will potentially serve as models for the complexes expected in solution during liquid-liquid separations of lanthanides by diamide extractants. Understanding the exact coordination environment of the metal from the solid-state studies reported herein will guide our interpretation of the future titration and X-ray scattering studies on metal complexation in solution.

Experimental Procedures

Synthetic Methods

All experimental solutions were prepared with methanol (VWR Chemicals BDH, ACS Grade, ≥99.8%), while 2-propanol (VWR Chemicals BDH, ACS Grade, ≥99.5%) and diethyl ether (Thermo Scientific, 99+% stabilized) were used as a co-solvent during crystallization. Lanthanum, cerium (III), holmium, and lutetium chloride salts were obtained from Strem Chemicals (99.9% metal basis); europium and erbium chloride salts were obtained from Alfa Aesar (99.99% REO); praseodymium chloride salt was obtained from Thermo Scientific (99.9% REO); neodymium, samarium, gadolinium, terbium, dysprosium, thulium, and ytterbium chloride salts were obtained from Sigma-Aldrich (99.99% metal basis). All lanthanide trichloride salts were acquired in their hydrate form. N,N,N',N'-tetramethylmalonamide was obtained from TCI America at >97.0% purity. All chemicals were used directly from the supplier without further purification.

Synthesis of $Ln(TMMA)_2Cl_3$ Ln = La-Dy

1.0 ml of 0.1M stock solution of $LnCl_3 \bullet xH_2O$ Ln = La-Dy in methanol was added to the bottom of a 20 ml glass scintillation vial with subsequent layering of 2 ml of 2-propanol. On top of the experimental mixture 0.2 ml / 0.6 ml / 1.0 ml of a 0.5M stock solution of *N,N,N',N'*-tetramethylmalonamide (TMMA) in methanol was layered depending on the desired Ln : TMMA molar ratio of 1:1, 1:3, or 1:5, respectively. Slow evaporation under ambient conditions resulted in the formation of viscous oils due to significant hygroscopicity of the formed complexes. To isolate crystalline material, the experimental solutions were placed in a container filled with indicating desiccant under a constant flow of nitrogen gas to minimize their exposure to moisture. When the reaction solutions were reduced to ~0.5 ml in volume, the scintillation vials were placed in a vacuum desiccator and the headspace was evacuated to avoid exposure to moisture. High quality crystals of $Ln(TMMA)_2Cl_3$ formed on the bottom of the vials within 24-48 hours inside the vacuum desiccator.

Synthesis of $[Ln(TMMA)_2(H_2O)_4]Cl_3 \bullet xH_2O$ *x* = 0,4 Ln = Ho-Lu

1.0 ml of 0.1M stock solution of $LnCl_3 \bullet xH_2O$ Ln = Ho-Lu in methanol was added to the bottom of a 20 ml glass scintillation vial with subsequent layering of 2 ml of 2-propanol. On top of the experimental mixture 0.2 ml / 0.6 ml / 1.0 ml of 0.5M stock solution of *N,N,N',N'*-tetramethylmalonamide (TMMA) in methanol was layered depending on the desired Ln : TMMA molar ratio of 1:1, 1:3, or 1:5, respectively. Slow evaporation under dry nitrogen with subsequent drying in the vacuum desiccator as described above again resulted in formation of viscous oils instead of crystalline materials, likely due to increased hygroscopicity of metal-organic complexes of the late lanthanides. These oils were re-dissolved in 1 ml of 2-propanol and then 2 ml of diethyl ether was added to each solution precipitating fine powders. The resulting suspension was mixed in with a few drops of mineral oil and placed back in the vacuum desiccator until the formation of crystalline $[Ln(TMMA)_2(H_2O)_4]Cl_3 \bullet xH_2O$ x = 0,4 was observed. A quick evaporation of diethyl ether in vacuum led to slow re-dissolution of the powders in remaining 2-propanol with subsequent re-crystallization within the mineral oil. Alternatively, such complexes could be obtained by directly mixing the intermediate oils with Parabar 10312 (Hampton Research) cryoprotective oil and leaving the mixture exposed to open air for several days, yet this approach yielded crystalline material only in the case of Ho and Yb reactions.

X-ray Diffraction

The crystals of $Ln(TMMA)_2Cl_3$ and $[Ln(TMMA)_2(H_2O)_4]Cl_3 \bullet xH_2O$ x = 0,4 were removed from the vials using a needle and placed directly into the Parabar 10312 (Hampton Research) cryoprotective immersion oil. A high-quality single crystal of each compound was isolated on a tip of a glass fiber mounted on a Bruker Quazar single crystal diffractometer equipped with a microfocus X-ray beam (Mo Kα; λ = 0.71073 Å) and an Apex II detector. The crystallographic frames were collected at 100K (Oxford Cryosystems Cryostream 700) with the Bruker APEXII software package. Peak intensities were corrected for Lorentz, polarization, background effects, and absorption effects using the APEX4 software. Initial structure solution was determined by intrinsic phasing and refined on the basis of F^2 for all unique data using the SHELXL version 5 program.[21] H atoms were placed with a riding model for all of the organic

functional groups. Summaries of the crystallographic refinements are provided in the Supporting Information. Individual CIFs including the structure factors have been deposited with the Cambridge Crystallographic Data Center under accession codes 2300738-2300751 for both $Ln(TMMA)_2Cl_3$ and $[Ln(TMMA)_2(H_2O)_4]Cl_3 \bullet xH_2O$ x = 0,4 compounds.

Powder X-ray diffraction patterns were collected on a Scintag diffractometer using nickel-filtered Cu Kα radiation (λ = 1.5418 Å), voltage 40 kV and current 40 mA. Samples were ground to fine powders using a mortar and pestle and run using zero background silica sample holder. Powder diffraction patterns were collected over the scan range of 5–50° 2θ, step size of 0.05°, and an exposure time of 1 second.

Vibrational Analysis

Solid-state compounds were analyzed by Fourier transform infrared (FT-IR) and Raman spectroscopy. FT-IR spectra were collected on an ATR accessory of a Nicolet Nexus 850 FT-IR spectrometer from 400-4000 cm^{-1} with a resolution of 2 cm^{-1}. Approximately 10-20 mg of the crystalline material was transferred directly into the ATR cavity and pressed down with the sampling arm. Particularly hygroscopic $[Ln(TMMA)_2(H_2O)_4]Cl_3 \bullet xH_2O$ x = 0,4 compounds were protected with Parabar 10312 immersion oil to avoid exposure to moisture, and thus, the IR spectra collected for these compounds did account for the mineral oil background.

Raman spectra were collected on a Renishaw inVia confocal Raman microscope with a Leica DM2700 series microscope using a 785 nm laser with a 1200/mm grating and a 532 nm laser with 2400/mm grating and a CCD detector. Each sample was isolated, mounted to a glass slide, and loaded onto the sample stage. Laser power was set at 10% (~50 mW) and the spectra were collected in the 100-1300 cm^{-1} range with each sample irradiated for an integration time of 1 s and automatically reiterated 100 times. Extended Raman scans were performed in the range 100-2000 cm^{-1} using variable laser power 10-50% with 10 s exposure time and 3-5 reiterations.

Results and Discussion

Solid-State Structure Analysis

The crystal structure of the isostructural series spanning lanthanum through dysprosium involves a lanthanide(III) metal center coordinated with two bidentate K^2-*N,N,N',N'*-tetramethylmalonamide ligands and three chloro ligands resulting in an overall charge-neutral complex with a formula of $Ln(TMMA)_2Cl_3$ where Ln = La – Dy, as shown in **Figure 1A**. The unit cell of $Ln(TMMA)_2Cl_3$ contains two molecular units that crystallize out in $P\bar{1}$ space group in the triclinic lattice for all La – Dy. Typical coordination numbers about the lanthanide metal center in the malonamide complexes reported to date range from 8 to 10, while the newly isolated compounds $Ln(TMMA)_2Cl_3$ show a coordination number of only 7.[22] Such an unsaturated coordination sphere of the lanthanides may explain the extreme hygroscopicity of the crystalline material, along with increasingly favorable hydration enthalpies of the lanthanide ions across the periodic series. The $Ln{-}O_{TMMA}$ bond distances of $Ln(TMMA)_2Cl_3$ across the lanthanide series show a monotonic decrease from 2.4774 Å (La) down to 2.3407 Å (Dy). The Ln−Cl bond lengths are elongated overall when compared to the $Ln{-}O_{TMMA}$ bond lengths yet displaying the

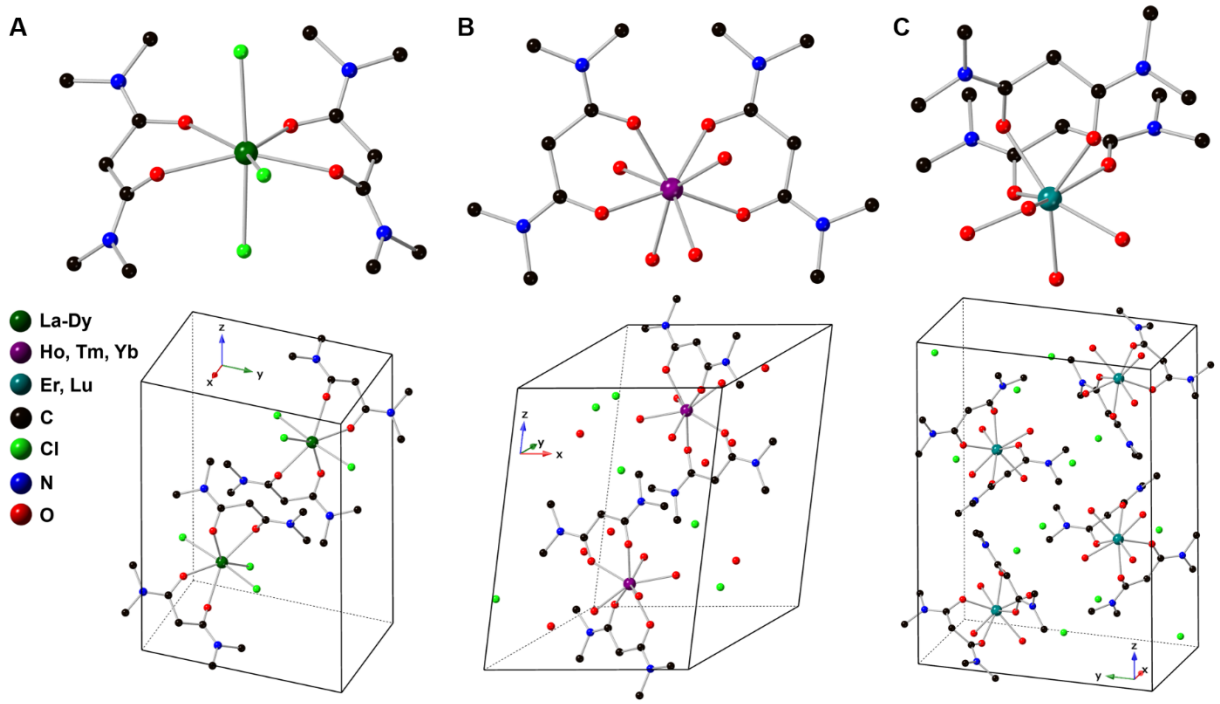

Figure 1. (**A**) Crystal structure and packing of $Ln(TMMA)_2Cl_3$ complex isostructural for La-Dy; (**B**) Crystal structure and packing of $[Ln(TMMA)_2(H_2O)_4]Cl_3 \bullet 4H_2O$ complex isostructural for Ho, Tm, and Yb; (**C**) Crystal structure and packing of $[Ln(TMMA)_2(H_2O)_4]Cl_3$ complex isostructural for Er and Lu. H atoms were omitted for clarity.

similar gradual decrease from 2.8025 Å (La) to 2.6704 Å (Dy), consistent with the contraction of the lanthanide ionic radius across the period.[23] The coordination geometry around the metal center is a distorted pentagonal bipyramid with two axially bound chloro ligands and both malonamides and the remaining chloro ligand bound in the equatorial plane. The spatial arrangement of TMMA ligands could be classified as *trans* due to the ligands taking up opposite sides of the coordination sphere of the lanthanide metal, yet the carbon backbones seem to be bent towards each other, forming a somewhat distorted C_{2v} symmetry. Such *trans* configuration of the malonamide ligands is particularly evident upon examining the packing of the unit cell, as shown in **Figure 1A**. Overall, the conformational geometry within the $Ln(TMMA)_2Cl_3$ series closely resembles the neodymium trisnitrato *N,N,N′,N′*-tetraethylmalonamide $Nd(TEMA)_2(NO_3)_3$ reported by Den Auwer *et al*., suggesting a common spatial arrangement of ligands around a metal center.[24]

The second structural series of compounds involves substitution of all three chloro ligands around the lanthanide metal center (Ho – Lu) with four aqua ligands, resulting in outer-sphere chloride complex formation, however the series can be subdivided into two distinct subgroups based on the number of non-coordinating water molecules in the crystalline lattice. The initial structural subgroup incorporates metal complexes containing holmium, thulium, and ytterbium that are coordinated by two bidentate *N,N,N',N'*-tetramethylmalonamide ligands, with four aqua ligands completing the remainder of the coordination sphere, resulting in an 8-coordinate $[Ln(TMMA)_2(H_2O)_4]^{3+}$ tripositive metal species, as shown in **Figure 1B**. The molecular complex is charge balanced with three chloride anions that are strongly H-bonded to the aqua ligands of the $[Ln(TMMA)_2(H_2O)_4]^{3+}$ and by four additional water molecules within the crystalline lattice, as shown in the unit cell packing for the $[Ln(TMMA)_2(H_2O)_4]Cl_3 \bullet 4H_2O$ compound (**Figure 1B**). The structural subgroup containing the remaining lanthanides, erbium and lutetium, displays a similar coordination environment around the Er/Lu metal center with two bidentate TMMA ligands and four aqua ligands and three outer-sphere chloride anions, resulting in an overall $[Ln(TMMA)_2(H_2O)_4]Cl_3$ complex (**Figure 1C**). The interstitial water molecules observed in the Ho, Tm, Yb complexes are absent

in the Er and Lu complexes, thus affecting the crystal packing with $[Ln(TMMA)_2(H_2O)_4]Cl_3 \bullet 4H_2O$ Ln = Ho, Tm, Yb compounds crystallizing in triclinic $P\bar{1}$ space group, while the $[Ln(TMMA)_2(H_2O)_4]Cl_3$ Ln = Er, Lu compounds take on a higher symmetry $P2_1/c$ space group of the monoclinic lattice.

Examination of bond lengths statistics shows a 0.04 Å drop in the $Ln{-}O_{TMMA}$ distances from $Dy(TMMA)_2Cl_3$ to $[Ho(TMMA)_2(H_2O)_4]Cl_3 \bullet 4H_2O$ following the chloro ligand substitution with water, resulting in $Ln{-}O_{TMMA}$ distances ranging from 2.3062 Å (Ho) to 2.2768 Å (Lu). The $Ln{-}O_{aqua}$ distances also gradually decrease from 2.3790 Å (Ho) to 2.3377 Å (Lu), as expected with the lanthanide contraction trend. The major difference between the two subgroups of $[Ln(TMMA)_2(H_2O)_4]Cl_3 \bullet xH_2O$ $x = 0,4$ besides the type of lanthanide and the stoichiometry of co-crystallized water molecules is the spatial arrangement of the diamide ligands around the metal center. In case of the tetrahydrate $[Ln(TMMA)_2(H_2O)_4]Cl_3 \bullet 4H_2O$ Ln = Ho, Tm, Yb compounds, the malonamide ligands occupy the opposite sides of the metal ion coordination sphere, similarly to the $Ln(TMMA)_2Cl_3$ series, yet the backbone of both ligands appears more planar, resembling D_{2h} symmetry across the metal center. This

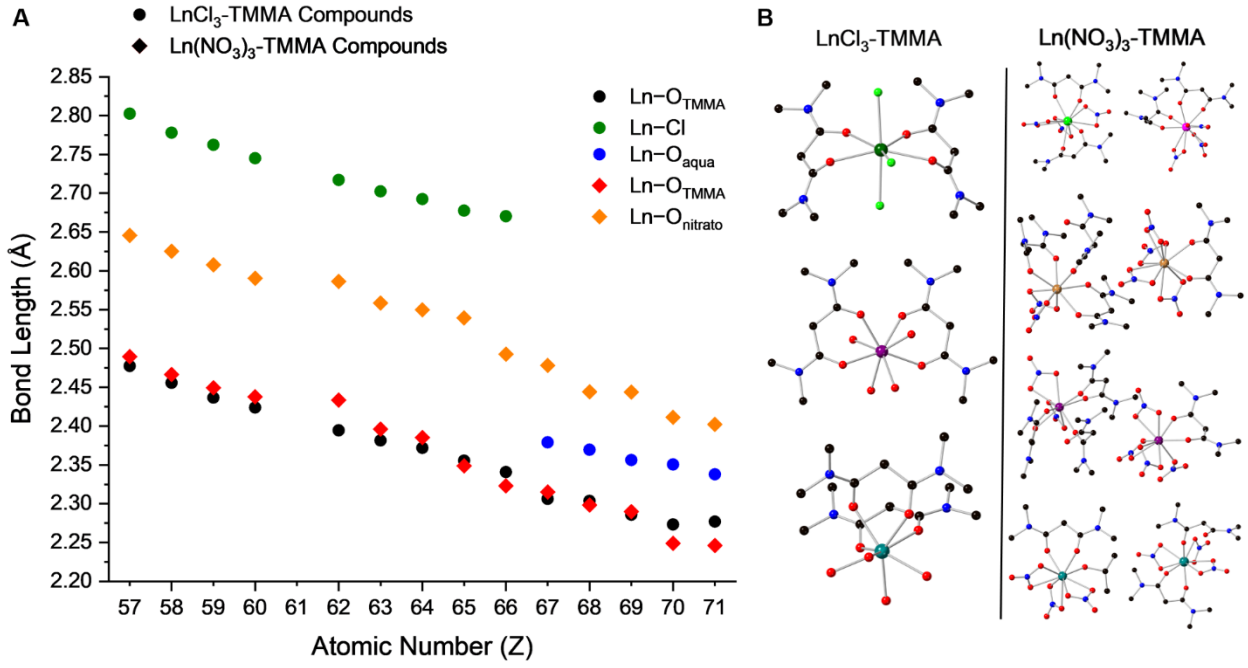

Figure 2. (**A**) Comprehensive comparison of the Ln-O/Cl_{ligand} bond distances across the $LnCl_3$-TMMA (spheres) and $Ln(NO_3)_3$-TMMA (diamonds) compound series; (**B**) Overview of molecular complexes for $LnCl_3$-TMMA and $Ln(NO_3)_3$-TMMA series.

conformational arrangement is rather different for $[Ln(TMMA)_2(H_2O)_4]Cl_3$ Ln = Er/Lu, where both TMMA ligands take up the same coordination hemisphere around the metal center, appearing to be *cis* with respect to each other, grouping the remaining aqua ligands on the opposite side of the metal. Interestingly, the *trans* and *cis* ligand arrangement for $[Ln(TMMA)_2(H_2O)_4]Cl_3 \bullet xH_2O$ x = 0,4 appears to hinge on the presence of interstitial water molecules and seems to be independent of the type of metal center, so we cannot rely on the trend in lanthanide contraction to explain these discrepancies.

The *trans* versus *cis* configuration of the malonamide ligands in the solid-state lanthanide complexes has first been noted by Parks *et al*. when comparing the crystal structures of La(*trans*-$TMMA)_2(NO_3)_3$ and Gd(*cis*-$TMMA)_2(NO_3)_3$.[15] To gain a fundamental understanding of this phenomenon, we recently conducted an in-depth study of the structural trends in the *N,N,N',N'*-tetramethylmalonamide nitrate complexes across the entirety of lanthanide series, isolating four families of solid-state compounds: Ln(*trans*-$TMMA)_2(NO_3)_3$ Ln = La-Nd, Sm; Ln(*cis*-$TMMA)_2(NO_3)_3$ Ln = Eu-Tb, Er; $[Ln(TMMA)_3(NO_3)_2][Ln(TMMA)(NO_3)_4]$ Ln = Dy-Tm; Ln(K^2-TMMA)(iPrOH)$(NO_3)_3$ and Ln(K^1-TMMA)(K^2-TMMA)$(NO_3)_3$ Ln = Yb, Lu (**Figure 2B**).[8] In addition to the spatial arrangement of ligands, we noted vast differences in ligand complexation for the later lanthanides including variability in ligand denticity and formation of heteroleptic anion-cation pairs in the $Ln(NO_3)_3$-TMMA series. Across both the $Ln(NO_3)_3$-TMMA and the $LnCl_3$-TMMA structural series reported herein, the $Ln{-}O_{TMMA}$ distances display a consistently contracting range from 2.48 Å to 2.26 Å (La-Lu) with the exception of the Sm, Yb, and Lu complexes. The samarium nitrate bis-malonamide complex appears to have an elongated $Sm{-}O_{TMMA}$ bond distance by 0.04 Å, compared to its trichloride counterpart, which interestingly coincides with the switch from the *trans* to the *cis* conformation of the TMMA ligand in the nitrate series (**Figure 2A**). The opposite bond length discrepancy is observed in the late lanthanides (Yb, Lu), where the $Ln(NO_3)_3$-TMMA complexes display 0.03 Å shorter $Yb/Lu{-}O_{TMMA}$ bond lengths, due to the change in dentisity of one of the malonamide ligands from bidentate to monodentate coordination. Aside from these

inconsistencies, the remaining survey of the bonds lengths appears to be compatible with the ionic radii of the coordinated ligands.

Structural diversity in the $Ln(NO_3)_3$-TMMA can be readily explained with the trend in decreasing ionic radii of the lanthanide cations, causing a switch from the *trans*-TMMA configuration for La-Sm to *cis*-TMMA configuration for Eu-Tb, with subsequent formation of anion-cation pairs for Dy-Tm, and finally the prevalence of monodentate K^1-TMMA binding mode for Yb-Lu. In comparison, the structural changes in the $LnCl_3$-TMMA appear to be driven more by the increase in favorable hydration enthalpies across the lanthanide period than the lanthanide contraction, favoring the displacement of chloro ligands for aqua ligands starting with a holmium complex.[25, 26] A complementary effect stems from the decrease in Ln−Cl bond distance across the lanthanide series, thus increasing the electron repulsion around the neighboring ligands, causing the chloro ligands to become more labile, resulting in the isolation of the tetraaqua complexes in the solid-state.[27, 28]

Vibrational Spectroscopy

The solid-state X-ray diffraction studies were paired with infrared and Raman spectroscopy to investigate the differences in vibrational signatures between the rare-earth chloride series. Overall, the IR and Raman spectra for $Ln(TMMA)_2Cl_3$ Ln = La-Dy and $[Ln(TMMA)_2(H_2O)_4]Cl_3 \bullet xH_2O$ x = 0,4 Ln = Ho-Lu respectively displayed identical vibrational features independent of the type of lanthanide metal present and despite conformational variations in the tetraaqua complexes (**Figure S17 S18 S33 S34)**. We thus chose a representative IR spectrum out of each series to provide a clearer visual distinction between the vibrational bands of each structural family. For example, the most noticeable difference is the presence of two intense bands at 3436 cm^{-1} and 3252 cm^{-1} in the IR spectrum of $[Ln(TMMA)_2(H_2O)_4]Cl_3 \bullet xH_2O$ x = 0,4 corresponding to the symmetric and asymmetric ν O-H of both the coordinated and interstitial water molecules, which are expectedly absent from the $Ln(TMMA)_2Cl_3$ spectrum (**Figure 3A**).

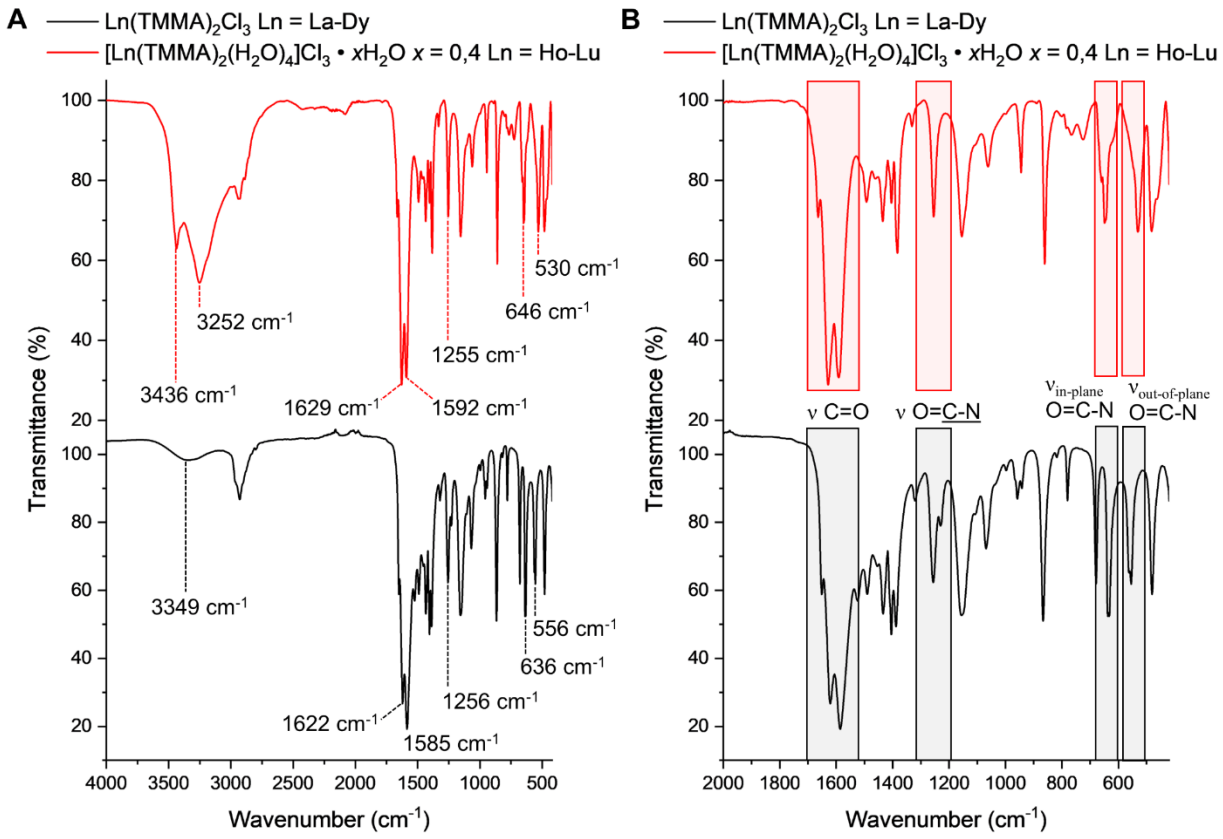

Figure 3. (**A**) Stacked infrared spectra for $Ln(TMMA)_2Cl_3$ (black trace) and $[Ln(TMMA)_2(H_2O)_4]Cl_3 \bullet xH_2O$ $x = 0,4$ (red trace) with the important vibrational features labelled; (**B**) Infrared spectra for $Ln(TMMA)_2Cl_3$ (black trace) and $[Ln(TMMA)_2(H_2O)_4]Cl_3 \bullet xH_2O$ $x = 0,4$ (red trace) enhanced in the 400-2000 cm^{-1} region.

In our previous work on lanthanide nitrate *N,N,N',N'*-tetramethylmalonamide complexes, we performed a detailed density functional theory frequency analysis to aid with vibrational band assignments, which can be helpful in this case due to similarities among the solid-state structures discussed above. Based on the previous DFT results, the vibrational bands around 2894-2968 cm^{-1} are common for both sets of solid-state compounds and coincide with ν C-H motion of the methyl and methylene groups on the malonamide ligands. Since the number and binding modes of coordinated malonamides is unchanged across $Ln(TMMA)_2Cl_3$ and $[Ln(TMMA)_2(H_2O)_4]Cl_3 \bullet xH_2O$ $x = 0,4$, both IR spectra dominated by a strong doublet at 1590 cm^{-1} and 1625 cm^{-1} that are assigned to the out-of-phase and in-phase motions of the C=O group (Amide I band), respectively. The bands at 1651 cm^{-1} ($Ln(TMMA)_2Cl_3$) and 1664 cm^{-1} ($[Ln(TMMA)_2(H_2O)_4]Cl_3 \bullet xH_2O$ $x = 0,4$) arise from individual carbonyl groups stretching in-phase with each other on a given ligand, while being out-of-phase with the carbonyl

groups on the opposing TMMA ligand (**Figure 3B**). Examining the vibrational signatures of the malonamide ligand, we note an appearance of the amide III band ν O=C-N in both spectra located at 1255 cm^{-1}, followed by the amide IV O=C-N deformation in the 635-646 cm^{-1} range, as well as the amide VI out-of-plane deformation of the amide functional group around 530-560 cm^{-1}. A detailed analysis of the remaining bands for $Ln(TMMA)_2Cl_3$ and $[Ln(TMMA)_2(H_2O)_4]Cl_3 \bullet xH_2O$ x = 0,4 can be found in **Table 1** and **Table 2**, respectively.

The complementary Raman spectra of the isolated compounds both show a prominent peak at 871 cm^{-1} for $Ln(TMMA)_2Cl_3$ and 865 cm^{-1} for $[Ln(TMMA)_2(H_2O)_4]Cl_3 \bullet xH_2O$ x = 0,4 corresponding to the ν_{sym} C-N-C (**Figure 4**). Interestingly, the diagnostic feature between the two families of compounds appears to be the asymmetric stretching of dimethyl substituted amide ν_{asym} C-N-C, a strong feature at 781 cm^{-1} in the spectrum of $Ln(TMMA)_2Cl_3$, that is completely absent from the spectrum of the tetraaqua complexes. The added advantage of Raman spectroscopy is the resolution of the low wavenumber region (100-400 cm^{-1}), where we typically expect the lanthanide-ligand vibrational modes. For example, the Raman spectrum of $Ln(TMMA)_2Cl_3$ shows vibrational features at 111 cm^{-1}, 138 cm^{-1}, and 169 cm^{-1} corresponding to the bending mode of either Cl-Ln-O_{TMMA} or Cl-Ln-Cl followed by Ln-Cl stretching modes at 199 cm^{-1} and 220 cm^{-1}, based on the reports by Oczko *et al*.[29] Hygroscopicity of lanthanide trichloro bismalonamides complexes is also evident based on an ingrowth of bands at 283 cm^{-1} and 316 cm^{-1} coinciding with the ν Ln-O_{aqua} stretching. It is likely that upon exposure to moisture the chloro ligands in $Ln(TMMA)_2Cl_3$ are substituted by aqua ligands resulting in the formation of $[Ln(TMMA)_2(H_2O)_4]Cl_3$, which we observe for the later lanthanides. Powder X-ray diffraction analysis confirms this assumption, since the finely ground powders of the $Ln(TMMA)_2Cl_3$ compounds readily take up water under ambient conditions, resulting in good agreement between the experimental PXRD patterns of $Ln(TMMA)_2Cl_3$ and the calculated pattern for $[Ln(TMMA)_2(H_2O)_4]Cl_3$ compounds, as shown in **Figure S15 S16**.

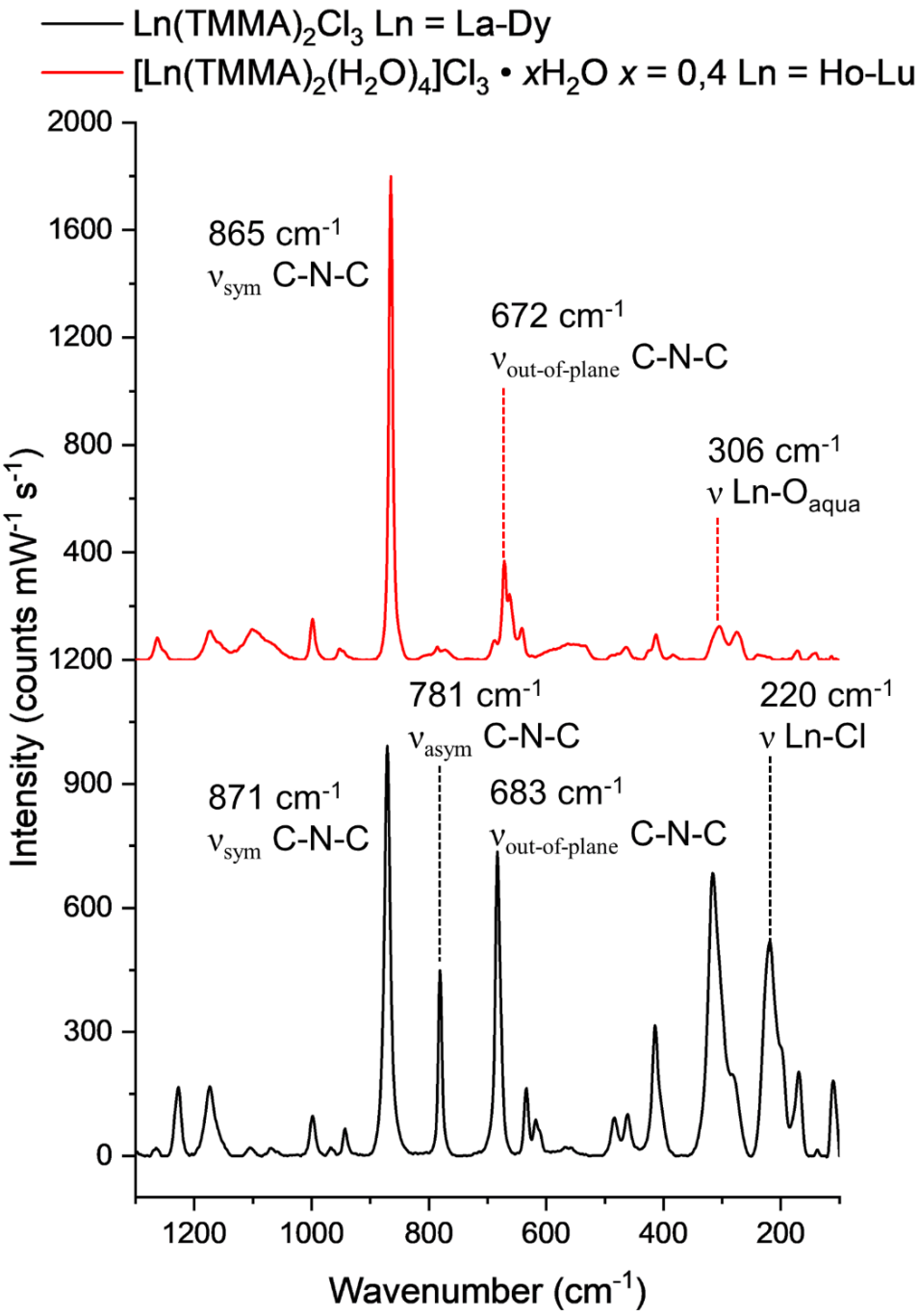

Figure 4. (**A**) Overlay of the Raman spectra for $Ln(TMMA)_2Cl_3$ (black trace) and $[Ln(TMMA)_2(H_2O)_4]Cl_3 \bullet xH_2O$ $x = 0,4$ (red trace).

Table 1. IR and Raman bands of $Ln(TMMA)_2Cl_3$ and their assignments.

$Ln(TMMA)_2Cl_3$			
IR	Raman	Assignment	Reference
	111 (m)	δ O-Ln-Cl or Cl-Ln-Cl	Oczko et al.[29]
	138 (vw)	δ O-Ln-Cl or Cl-Ln-Cl	Oczko et al.[29]
	169 (m)	δ O-Ln-Cl or Cl-Ln-Cl	Oczko et al.[29]
	199 (m, sh)	ν Ln-Cl	Oczko et al.[29]
	220 (s)	ν Ln-Cl	Oczko et al.[29]
	283 (m, sh)	ν Ln-O_{aqua}	Oczko et al.[29]
	316 (s)	ν Ln-O_{aqua}	Oczko et al.[29]
403 (s)	414 (s)	ν C-C skeletal	Socrates[30]
	461 (w)	ν C-C skeletal	Socrates[30]
480 (m)	484 (w)	ν C-C skeletal	Socrates[30]
556 (m)		Amide VI, out-of-plane N-C=O def	Socrates[30]
636 (s)	635 (m)	Amide IV, N-C=O def	Bellamy[31]
680 (m)	683 (vs)	$\delta_{out\text{-}of\text{-}plane}$ H_3C-N-CH_3	Kravchuk et al.[8]
781 (m)	781 (s)	ν_{asym} C-N-C	Socrates[30]
866 (s)	871 (vs)	ν_{sym} C-N-C	Socrates[30]
943 (w, sh)	943 (w)	ρ CH_2	De Beukeleer and Desseyn[32]
959 (w)		ρ CH_2	De Beukeleer and Desseyn[32]
	999 (w)	δ CH_3	Kravchuk et al.[8]
1068 (w)		ρ CH_3	Socrates[30]
1154 (m)	1174 (m)	ν_{asym} O=C-CH_2-C=O backbone	Socrates[30]
1231 (w, sh)	1227 (m)	$\delta_{in\text{-}plane}$ C-N-C	Kravchuk et al.[8]
1256 (m)		Amide III, ν O=C-N	Bellamy[31]
1388 (s)		ν N-CH_3	Bellamy[31]
1404 (s)		O=C-CH_2-C=O def coupled to ν C=O	Kravchuk et al.[8]
1433 (m)		O=C-CH_2-C=O def coupled to ν C=O	Kravchuk et al.[8]
1490 (m)		$\delta_{in\text{-}plane}$ N-C=O	Kravchuk et al.[8]
1585 (vs)		ν C=O out-of-phase	Kravchuk et al.[8]
1622 (vs)		$\nu_{in\text{-}phase}$ C=O, *trans*-TMMA out-of-phase	Kravchuk et al.[8]
1651 (m)		$\nu_{in\text{-}phase}$ C=O, *trans*-TMMA in-phase	Kravchuk et al.[8]
2894 (w, sh)		ν C-H (CH_2)	Bellamy[31]
2929 (w)		ν C-H (CH_2)	Bellamy[31]
2968 (w, sh)		ν C-H (CH_3)	Bellamy[31]
3349 (vw)		ν O-H	Oczko et al.[29]

Table 2. IR and Raman bands of $[Ln(TMMA)_2(H_2O)_4]Cl_3 \bullet xH_2O$ $x = 0,4$ and their assignments.

$[Ln(TMMA)_2(H_2O)_4]Cl_3 \bullet xH_2O$ $x = 0,4$			
IR	Raman	Assignment	Reference
	120 (vw)	ν Ln-O=C out-of-phase	Kravchuk et al.[8]
	150 (vw)	ν Ln-O=C in-phase	Kravchuk et al.[8]
	225 (vw)	δ O-Ln-O	Oczko et al.[29]
	242 (vw)	ν Ln-O_{aqua}	Oczko et al.[29]
	277 (m)	ν Ln-O_{aqua}	Oczko et al.[29]
	306 (m)	ν Ln-O_{aqua}	Oczko et al.[29]
412 (vs)	413 (m)	ν C-C skeletal	Socrates[30]
	427 (w, sh)	ν C-C skeletal	Socrates[30]
463 (m, sh)	464 (w)	ω H_2O-Ln	Oczko et al.[29]
483 (m)	488 (w, sh)	ν C-C skeletal	Socrates[30]
531 (m)	530 (w)	Amide VI, out-of-plane N-C=O def	Socrates[30]
620 (w, sh)		$\delta_{out\text{-}of\text{-}plane}$ H_3C-N-CH_3	Kravchuk et al.[8]
646 (m)	643 (m)	Amide IV, N-C=O def	Bellamy[31]
	664 (m)	ν_{asym} C-CH_2-C	Kravchuk et al.[8]
	672 (s)	$\delta_{out\text{-}of\text{-}plane}$ H_3C-N-CH_3	Kravchuk et al.[8]
	687 (m)	$\delta_{out\text{-}of\text{-}plane}$ H_3C-N-CH_3	Kravchuk et al.[8]
	716 (m)	ω CH_2	Kravchuk et al.[8]
727 (w)		Parabar oil	This Work
768 (w)		ν_{sym} C-CH_2-C	Kravchuk et al.[8]
862 (s)	865 (vs)	ν_{sym} C-N-C	Socrates[30]
946 (m)		ρ CH_2	De Beukeleer and Desseyn[32]
	999 (m)	δ CH_3	Kravchuk et al.[8]
1061 (m)	1063 (w)	ρ CH_3	Socrates[30]
1155 (s)	1157 (m, sh)	ν_{asym} O=C-CH_2-C=O backbone	Socrates[30]
	1173 (m)	ν_{asym} O=C-CH_2-C=O backbone	Socrates[30]
	1229 (vw)	$\delta_{in\text{-}plane}$ C-N-C	Kravchuk et al.[8]
1255 (s)	1263 (w)	Amide III, ν O=C-N	Bellamy[31]
1383 (s)		ν N-CH_3	Bellamy[31]
1405 (m)		O=C-CH_2-C=O def coupled to ν C=O	Kravchuk et al.[8]
1436 (m)		O=C-CH_2-C=O def coupled to ν C=O	Kravchuk et al.[8]
1492 (m)		$\delta_{in\text{-}plane}$ N-C=O	Kravchuk et al.[8]
1592 (vs)		ν C=O out-of-phase	Kravchuk et al.[8]
1629 (vs)		$\nu_{in\text{-}phase}$ C=O, *trans*-TMMA out-of-phase	Kravchuk et al.[8]
1664 (m, sh)		$\nu_{in\text{-}phase}$ C=O, *trans*-TMMA in-phase	Kravchuk et al.[8]
2927 (m)		ν C-H (CH_2)	Bellamy[31]
3252 (s)		ν_{asym} O-H	Oczko et al.[29]
3436 (s)		ν_{sym} O-H	Oczko et al.[29]

Conclusion

Crystallization reactions between the rare-earth chloride salts and *N,N,N′,N′*-tetramethylmalonamide resulted in isolation of two related families of compounds $Ln(TMMA)_2Cl_3$ for lanthanum through dysprosium and $[Ln(TMMA)_2(H_2O)_4]Cl_3 \bullet xH_2O$ $x = 0,4$ for holmium through lutetium. The major difference between the solid-state structure stems from the inner-sphere coordination of chloride in the case of early and middle lanthanides, with a substitution of the chloro ligands for aqua ligands for the late lanthanides due to increasingly favorable hydration enthalpies and lability of the chloro ligands. Extensive comparison of the chloro series of molecules has been made to the lanthanide nitrate malonamide series, showing significant differences in the structural chemistry across the rare-earth period, despite similarities in synthetic preparations. IR and Raman spectroscopy was employed to compare and contrast vibrational signatures of between $Ln(TMMA)_2Cl_3$ and $[Ln(TMMA)_2(H_2O)_4]Cl_3 \bullet xH_2O$ $x = 0,4$. The synthesis and structural characterization of both the chloride and nitrate lanthanide malonamide complexes serves as a foundational step to correlating the solid state structures of these complexes with the solution phase structures and speciation encountered in the liquid-liquid extraction systems that they are employed in highlighting a close interplay between the lanthanide contraction, sterics, and solvation thermodynamics.

Supporting Information

The Supporting Information section is available free of charge and includes detailed crystallographic information, IR and Raman spectra for each compound, powder X-ray diffraction patterns.

Acknowledgments

This work was conducted at Argonne National Laboratory, operated by UChicago Argonne LLC for the United States Department of Energy (U.S. DOE), and supported by the U.S. DOE Office of Science, Office of Basic Energy Sciences, Chemical Sciences Geological and Biosciences Division, under Contract DE-AC02-06CH11357.

References

1. Gannaz, B., et al., *Extraction of Lanthanides(III) and Am(III) by Mixtures of Malonamide and Dialkylphosphoric Acid.* Solvent Extraction and Ion Exchange, 2007. **25**(3): p. 313-337.
2. Berthon, L., et al., *DIAMEX PROCESS FOR MINOR ACTINIDE PARTITIONING: HYDROLYTIC AND RADIOLYTIC DEGRADATIONS OF MALONAMIDE EXTRACTANTS.* Separation Science and Technology, 2001. **36**(5-6): p. 709-728.
3. Heres, X., et al., *Extractant separation in DIAMEX-SANEX process*. 2007, United States: American Nuclear Society - ANS.
4. Aneheim, E., et al., *Development of a Novel GANEX Process*, in *Nuclear Energy and the Environment*. 2010, American Chemical Society. p. 119-130.
5. Taylor, R., et al., *The EURO-GANEX Process: Current Status of Flowsheet Development and Process Safety Studies.* Procedia Chemistry, 2016. **21**: p. 524-529.
6. Ellis, R.J. and M.R. Antonio, *Coordination Structures and Supramolecular Architectures in a Cerium(III)–Malonamide Solvent Extraction System.* Langmuir, 2012. **28**(14): p. 5987-5998.
7. Ellis, R.J., et al., *Periodic Behavior of Lanthanide Coordination within Reverse Micelles.* Chemistry – A European Journal, 2013. **19**(8): p. 2663-2675.
8. Kravchuk, D., et al., *Structural Trends and Vibrational Analysis of N, N, N', N'-Tetramethylmalonamide Complexes Across the Lanthanide Series.* ChemRxiv, 2023.
9. Aspinall, H.C., *Chemistry of the f-Block Elements*. 2001: Taylor & Francis.
10. Castellano, E.E. and R.W. Becker, *Structural studies of addition compounds of lanthanides with organic ligands. II. Lanthanum hexafluorophosphate and N,N,N',N'-tetramethylmalonamide.* Acta Crystallographica Section B, 1981. **37**(11): p. 1998-2001.
11. Kannan, S. and G. Ferguson, *Synthesis and Crystal Structure of (μ-Malonanilide-O,O')bis[bis(dibenzoylmethanato)dioxouranium(VI)]: A New Coordination Mode of the Malonamide Ligand.* Inorganic Chemistry, 1997. **36**(8): p. 1724-1725.
12. Y. S. Chan, G., et al., *Solvent extraction of metal ions from nitric acid solution using N,N'-substituted malonamides. Experimental and crystallographic evidence for two mechanisms of extraction, metal complexation and ion-pair formation.* Journal of the Chemical Society, Dalton Transactions, 1997(4): p. 649-660.
13. B. Iveson, P., et al., *Structural studies of lanthanide complexes with new hydrophobic malonamide solvent extraction agents †.* Journal of the Chemical Society, Dalton Transactions, 1999(20): p. 3605-3610.
14. Lumetta, G.J., et al., *Deliberate Design of Ligand Architecture Yields Dramatic Enhancement of Metal Ion Affinity.* Journal of the American Chemical Society, 2002. **124**(20): p. 5644-5645.
15. Parks, B.W., et al., *Solution and Structural Investigations of Ligand Preorganization in Trivalent Lanthanide Complexes of Bicyclic Malonamides.* Inorganic Chemistry, 2006. **45**(4): p. 1498-1507.
16. Tyumentsev, M.S., et al., *Coordination of Trivalent Lanthanides with Bismalonamide Ligands: Implications for Liquid–Liquid Extraction.* European Journal of Inorganic Chemistry, 2017. **2017**(37): p. 4285-4298.
17. Modolo, G., et al., *DIAMEX Counter-Current Extraction Process for Recovery of Trivalent Actinides from Simulated High Active Concentrate.* Separation Science and Technology, 2007. **42**(3): p. 439-452.
18. Baron, P., et al. *Separation of the minor actinides: the DIAMEX-SANES concept*. in *Global 2001 international conference on: ''back-end of the fuel cycle: from research to solutions''*. 2001. France.

19. Street, K., Jr. and G.T. Seaborg, *The Separation of Americium and Curium from the Rare Earth Elements.* Journal of the American Chemical Society, 1950. **72**(6): p. 2790-2792.
20. Diamond, R. and K. Street Jr, *An ion-exchange study of possible hybridized 5f bonding in the actinides1.* Journal of the American chemical society, 1954. **76**(6): p. 1461-1469.
21. Sheldrick, G., *SHELXT - Integrated space-group and crystal-structure determination.* Acta Crystallographica Section A, 2015. **71**(1): p. 3-8.
22. Drew, M.G.B., et al., *Crystal structure of [Yb(L(NO3)2(H2O)2](NO3), L = bromo-N,N,N',N'-tetraethylmalonamide.* Journal of Chemical Crystallography, 2000. **30**(7): p. 455-458.
23. Goldschmidt, V., *Skrifter Norske Videnskaps-Akad.* Oslo I, Mat-Naturvidensk Kl, 1926. **8**(2).
24. Den Auwer, C., et al., *Crystallographic, X-ray Absorption, and IR Studies of Solid- and Solution-State Structures of Tris(nitrato) N,N,N',N'-Tetraethylmalonamide Complexes of Lanthanides. Comparison with the Americium Complex.* Inorganic Chemistry, 2000. **39**(7): p. 1487-1495.
25. Bertha, S.L. and G.R. Choppin, *Hydration thermodynamics of the lanthanide ions.* Inorganic Chemistry, 1969. **8**(3): p. 613-617.
26. Marcus, Y., *A simple empirical model describing the thermodynamics of hydration of ions of widely varying charges, sizes, and shapes.* Biophysical Chemistry, 1994. **51**(2): p. 111-127.
27. Rodríguez-Rodríguez, A., et al., *Definition of the Labile Capping Bond Effect in Lanthanide Complexes.* Chemistry – A European Journal, 2017. **23**(5): p. 1110-1117.
28. Zhang, J. and M. Dolg, *Labile Capping Bonds in Lanthanide(III) Complexes: Shorter and Weaker.* The Journal of Physical Chemistry A, 2015. **119**(4): p. 774-780.
29. Oczko, G., et al., *Comparison of the spectroscopic behaviour of single crystals of lanthanide halides (X = Cl, Br).* Journal of Alloys and Compounds, 2004. **380**(1): p. 327-336.
30. Socrates, G., *Infrared and Raman Characteristic Group Frequencies: Tables and Charts*. 2004: Wiley.
31. Bellamy, L.J., *The Infrared Spectra of Complex Molecules: Volume Two Advances in Infrared Group Frequencies*. 1980: Springer Netherlands.
32. De Beukeleer, S.H.J. and H.O. Desseyn, *Vibrational analysis of some transition metal complexes with deprotonated and neutral malonamide.* Spectrochimica Acta Part A: Molecular Spectroscopy, 1994. **50**(14): p. 2291-2309.